Acta Crystallographica Section D
Biological Crystallography
ISSN 0907-4449

Cryogenic (<20 K) helium cooling mitigates radiation damage to protein crystals

Unmesh Chinte,[a] Binal Shah,[a] Yu-Sheng Chen,[b,c] A. Alan Pinkerton,[b] Constance A. Schall[a] and B. Leif Hanson[b]*

[a]Department of Chemical and Environmental Engineering, University of Toledo, USA, [b]Department of Chemistry, University of Toledo, USA, and [c]Bio-CARS, Advanced Photon Source, Argonne National Laboratory, USA

Correspondence e-mail: leif.hanson@gmail.com

Received 8 June 2006
Accepted 31 January 2007

In experiments conducted at the Bio-CARS beamline 14-BM-C (APS, Argonne National Laboratory, USA), *Streptomyces rubiginosus* D-xylose isomerase (EC 5.3.1.5) crystals were used to test the effect of cryogen temperature on radiation damage. Crystals cooled using a helium cryostat at an 8 K set temperature consistently showed less decay in the signal-to-noise ratio, $\langle I/\sigma(I)\rangle$, and in average intensity, $\langle I\rangle$, compared with those cooled with a nitrogen cryostat set to 100 K. Multiple crystals grown using ammonium sulfate as precipitant were used at each cryostat set temperature and comparisons were made for crystals of similar size and diffraction resolution. Maximum resolution for the crystals was 1.1–1.3 Å, with He at <20 K extending the lifetime of the high-resolution data by >25% compared with crystals cooled with N_2 at 100 K.

1. Introduction

Cryocrystallography has played an integral role in the success of structural biology (Hope, 1988; Rodgers, 1994; Garman & Schneider, 1997; Garman, 1999; Garman & Owen, 2006). It has allowed the development and proliferation of phasing techniques that use exhaustive sampling of the diffraction from a single crystal, such as multi-wavelength or single-wavelength anomalous dispersion (MAD or SAD) techniques, or the measurement of ultrahigh-resolution (better than 1.1 Å) diffraction data sets. By measuring data at cryogenic temperatures, where the solvent inside and outside the crystal forms a glassy matrix, radiation-induced free radicals are restricted in their migration through the crystalline biological material.

However, current crystal-cooling regimes have proven to be inadequate for the challenges posed by the high-flux X-ray sources available at third-generation synchrotrons. By illuminating the crystals with more X-ray photons in a shorter time period, radiation damage manifests rapidly and can prevent the collection of sufficiently complete data to solve the structure of a new protein using MAD or SAD phasing or for the unambiguous determination of all atomic positions in an ultrahigh-resolution structure, thus limiting the throughput of these incredibly powerful structural biology tools. To maximize the use of these sources, it is necessary to minimize the damage induced by X-radiation in crystalline samples. The question prompting this study is whether cryogenics and cryocrystallographic techniques can be improved to further abate the damage that is induced by radiation exposure.

Numerous studies have detailed the various mechanisms involved in radiation damage and explored possible mitigation of radiation damage (Nave, 1995; Sharpatyi, 1995; Garman & Nave, 2002; O'Neill *et al.*, 2002; Nave & Garman, 2005).

Radical formation arising from direct beam interaction is termed 'primary radiation damage'. The formation of ions and radicals and the diffusion or migration and subsequent reactions of these species with the protein molecule is termed 'secondary damage'. Radical formation is a consequence of homolysis or heterolysis of covalent bonds in either the solvent or the protein molecule itself. The most plentiful chemical on a molar basis in protein crystals is water. Exposure to ionizing X-rays causes radiolysis of water, resulting in the formation of free radicals and charged species; *e.g.* $H^{\cdot}$, $OH^{\cdot}$, e^{-}_{aq} and H_3O^{+} (Turner, 1992). These small highly mobile moieties can then attack the protein, causing further damage. Primary damage is strictly dose-dependent and is independent of the temperature of data collection. Secondary damage is dependent upon the kinetics, diffusion and mobility of reactive species; thus, subsequent reaction with the protein is expected to be temperature-dependent.

The damage to the protein molecule may be site-specific (Burmeister, 2000; Ravelli & McSweeney, 2000; Weik *et al.*, 2000, 2001, 2002; O'Neill *et al.*, 2002). Weik *et al.* (2001) analysed damage to disulfide bonds in *Torpedo californica* acetylcholinesterase (TCAChE) crystals at 100 K (below the glass-transition temperature, T_g, of the solvent) and 155 K (close to the T_g of the solvent). The electron-density maps in the region of the disulfide bonds were examined from data measured at 100 and 155 K. Bond damage was more extensive at 155 K than at 100 K and was attributed to increased radical mobility at 155 K. In these crystals, individual disulfide bonds had different radiation-sensitivity. Weik and coworkers suggested that this could be attributable to the solvent accessibility (free-radical accessibility) of the disulfide bonds, where solvent-accessible bonds exhibited greater damage.

As primary damage is only dose-dependent, it cannot be minimized without reducing the total photon flux or changing the crystal properties. Secondary damage depends on the mobility and reactions of the reactive species and therefore may be mitigated by the use of radical scavengers (Murray & Garman, 2002) or lower data-collection temperatures, the latter being the focus of our study. In contrast with the method of Weik *et al.* (2001), where site-specific damage was tracked, our approach has been to examine the manifestations of radiation damage as seen in the diffraction data. Our chosen methodology is to follow the changes in diffraction parameters that adversely affect the quality of the data (Hanson *et al.*, 2002), providing a result that may be applied to a variety of crystals and data-collection conditions.

Manifestations of radiation damage in diffraction data can appear as increased mosaicity, changes in unit-cell parameters or a decrease in overall intensity and in the signal-to-noise ratio $I/\sigma(I)$ (Teng & Moffat, 2000, 2002; Ravelli *et al.*, 2002; Murray & Garman, 2002; Sliz *et al.*, 2003; Schulze-Briese *et al.*, 2005). Heretofore, no single metric has been found to uniformly reflect the effects of increasing radiation dose on a crystal. However, although mosaicity and unit-cell volume changes can adversely affect the diffraction, the loss of signal can preclude the solution of a structure. For this reason the signal-to-noise ratio, $\langle I/\sigma(I)\rangle$, was used in these studies as the principal metric of radiation damage, although the other parameters were also measured and changes noted.

The most common method of cryogenic data collection uses a cryostat that bathes the crystal in a flowing nitrogen-gas stream at a temperature of ~100 K. The use of helium for data collection is an alternative. Helium has a lower boiling point (4 K) than nitrogen (77 K), which permits colder gas-stream temperatures with concomitant lower data-collection temperatures. We have previously reported the use of a helium cryostream for mitigating effects of radiation damage and have shown improvements in diffraction resolution and intensities for crystals of various proteins (Hanson *et al.*, 1999, 2001, 2002, 2003). In these earlier studies, comparisons were limited by crystal availability; only one crystal in the helium and nitrogen stream was used for each macromolecule. Here, we report systematic experiments on multiple *Streptomyces rubiginosus* D-xylose isomerase (EC 5.3.1.5) crystals grown using the same crystallization conditions, cryoprotected using the same protocol and flash-cooled using the same method. Data were measured at two stream temperatures, with cryostat settings of 8 K (helium) and 100 K (nitrogen), and diffraction statistics were compared for crystals diffracting to similar resolution.

2. Materials and methods

2.1. Crystallization

The crystallization protocol used for these studies deviated somewhat from that used in our previous studies (Hanson *et al.*, 2002). D-Xylose isomerase (XI) for these studies was purchased from Hampton Research (HR7-100). The protein crystal suspension was dialyzed against 100 m*M* Tris–HCl buffer pH 8.0 with 10 m*M* EDTA to remove metal ions. The solution was then exchanged for a final buffer concentration of 100 m*M* Tris–HCl pH 8.0 with 10 m*M* $MgCl_2$. The protein was crystallized at 277 K using ammonium sulfate as precipitant. Crystals were grown in hanging drops with 52 mg ml^{-1} protein and 10%(*w*/*v*) ammonium sulfate. The concentration of ammonium sulfate and buffer in the well solution matched the initial concentration in the crystallizing drop. Crystals appeared in less than 24 h and grew to maximum dimensions (~0.5 mm on the longest edge) in about 2 d.

Two criteria were used to establish matched crystals: size and diffraction resolution. Two of the dimensions of the crystals were similar, with the third dimension being about half of the other two (*e.g.* a typical crystal size was ~0.5 × 0.5 × 0.25 mm for nominal 0.4–0.5 mm crystals). Two different size classes of crystals were used for data collection: 0.4–0.5 mm and 0.1–0.2 mm in the longest dimension. The 0.4–0.5 mm crystals diffracted to ~1.1 Å (*i.e.* the margin of the detector), while 0.1–0.2 mm crystals diffracted to 1.3–1.4 Å resolution.

2.2. Cryoprotection

Glycerol was used as the cryoprotectant. Glycerol solutions were made in 5%(*v*/*v*) increments while maintaining the buffer concentration at 100 m*M* Tris–HCl and 10 m*M* $MgCl_2$.

The ammonium sulfate concentration in the glycerol–buffer–salt mixture was maintained at 20%(*w*/*v*), which differed from that used in our previous studies (Hanson *et al.*, 2002). Crystals were serially passed from well to well on a nine-well depression plate with 1 min soaks through 5, 10 and 15% glycerol solutions. After serial passage, all crystals used in this study were flash-cooled by plunging into liquid N_2. Crystals were then transferred from liquid N_2 onto the goniometer head under the cold gas cryostat using cryotongs.

2.3. Data-collection strategy

Data collection at a set temperature of 100 K was carried out using a cold nitrogen stream produced by an Oxford Instruments Cryojet. The crystal was positioned about 1.0 cm from the nozzle tip during nitrogen data collection. From previous studies using an Oxford 600 Cryostream (Chinte, 2006), we have determined that the temperature varies in the radial direction from the center of the cold stream in an approximately broad parabolic fashion (the stream temperature rises by ∼25–30 K at a 3 mm radial distance from the center). Therefore, the cold stream was aligned so that the coldest part of the stream was at the crystal position. The temperature at the crystal position (∼2 mm from the cold-stream center) was measured as ∼112 K using an E-type (chromel–constantan) thermocouple in noncoaxial orientation to the cold stream. For data measurement below 100 K, the open-flow helium Pinkerton Device (Hardie *et al.*, 1998) was used at a set temperature of 8 K. The crystal was positioned in the coldest part of the stream. During helium data collection, the crystal was positioned about 2 mm away from the nozzle tip. The helium stream delivered by the Pinkerton device is only 2 mm wide, making centering of the crystal in the stream crucial and the single greatest cause of crystal loss. The temperature at the crystal position at a set temperature of 8 K was measured to be ∼12 K using a chromel–AuFe 0.07% thermocouple in coaxial orientation with the connecting wires shrouded inside ceramic beads connected to a LakeShore Cryotonics 330 controller (Westerville, OH, USA) with the manufacturer's calibration curve.

Diffraction data were measured at BioCARS (APS beamline 14-BM-C) with an ADSC Quantum 315 detector and 0.9 Å X-radiation. The crystal-to-detector distance was 150 mm and the 2θ offset was 0°, yielding a resolution of about 1.08 Å at the margin and 0.95 Å at the corner of the detector. The measurement time for each frame was 2 s for all runs. The beam at 14-BM-C was not attenuated. An initial data set consisting of ten frames with 1° frame width was measured. The same portion of the crystal was then re-exposed to the beam ('burned') for 10 min with the detector covered. The detector was uncovered and data were measured again on the same crystal portion as the initial set. Crystal 'burn' and data-measurement cycles were repeated six times. Partial data sets were measured to maximize the number of crystals that could be sampled (finding well diffracting crystals with similar limits of resolution proved more problematic than originally antici-

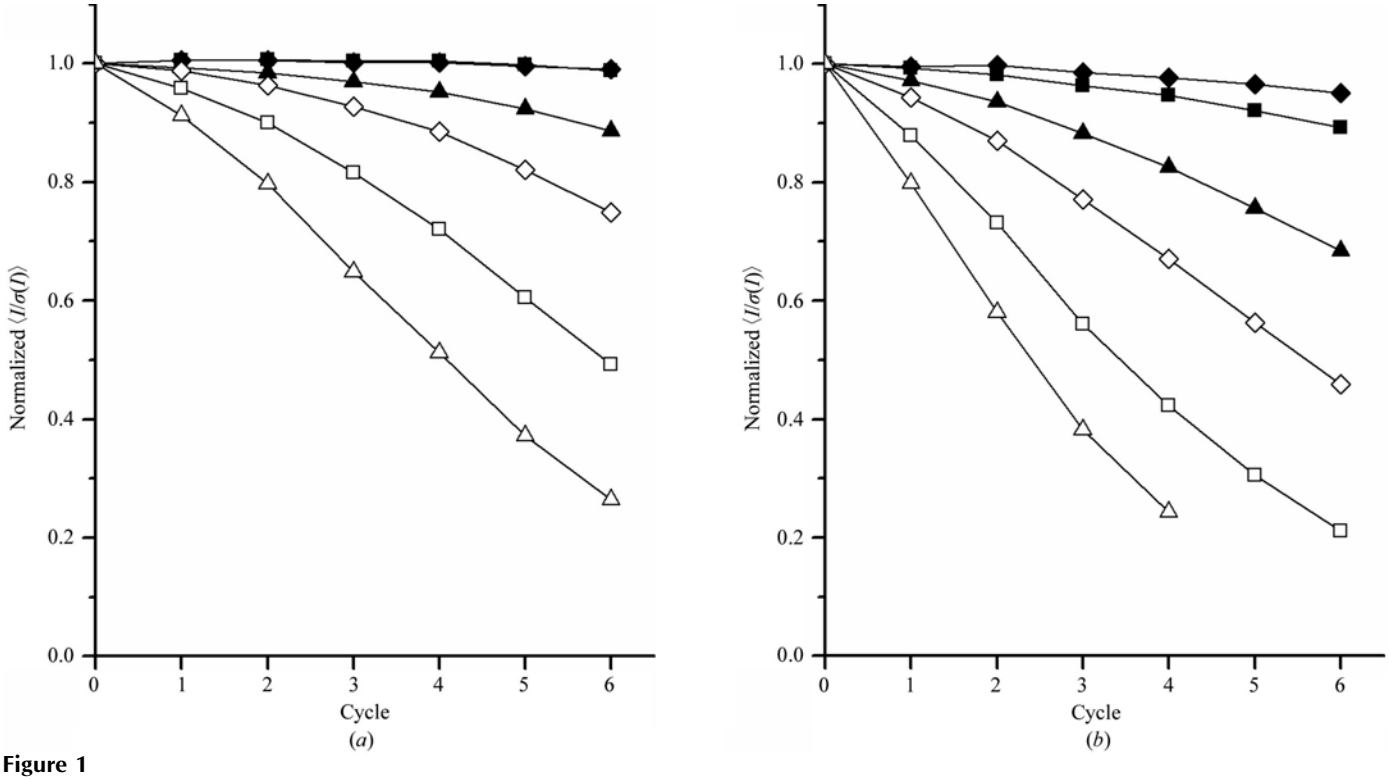

Figure 1
$\langle I/\sigma(I)\rangle$ over 10° wedges, normalized to the initial values in each $\sin\theta/\lambda$ section, *versus* number of cycles for (*a*) a 0.1–0.2 mm crystal cooled in an 8 K helium stream, (*b*) a 0.1–0.2 mm crystal cooled at 100 K. The data for $\langle I/\sigma(I)\rangle \geq 1.5$ are shown in $\sin\theta/\lambda$ shells: 0–0.1 $Å^{-1}$ (to 5 Å; closed diamonds), 0.1–0.15 $Å^{-1}$ (5.0–3.3 Å; closed squares), 0.15–0.2 $Å^{-1}$ (3.3–2.5 Å; closed triangles), 0.2–0.25 $Å^{-1}$ (2.5–2.0 Å; open diamonds), 0.25–0.3 $Å^{-1}$ (2.0–1.7 Å; open squares), 0.3–0.365 $Å^{-1}$ (1.7–1.3 Å; open triangles). Helium data show consistently less decay when the same $\sin\theta/\lambda$ shells are compared.

pated) and to minimize scaling issues found with measuring complete data.

2.4. Radiation dose

The radiation dose absorbed by the crystals was calculated using the *RADDOSE* program (Murray *et al.*, 2004). The program calculates the dose based on the beam parameters, exposure time, crystal properties and the type of solvent present in the crystal. The beam width was 200 × 200 µm and the total exposure time of the crystal in the beam was 3740 s during the course of the experiments. The APS at the time of data measurement was in 'top-off' mode, thus there was minimal variation in the ionization-chamber measurements of flux. The photon flux at the crystal position was ∼9.75 × 10^{10} photons s^{-1} [2.4 × 10^{12} photons s^{-1} mm^{-2}] for the 200 µm aperture as measured using a calibrated ion chamber for the 0.9 Å wavelength. Other input parameters to the program included the unit-cell parameters (a = 92, b = 98, c = 101 Å), solvent content (55%), number of amino-acid residues (388), number of monomers in the unit cell (eight) and the ammonium sulfate concentration in the solvent (1.5 *M*). The radiation dose absorbed by each of the crystals at the end of data-collection cycles calculated using the *RADDOSE* program was 3.5 × 10^6 Gy (Garman, personal communication) for each crystal, compared with the Henderson limit of 2 × 10^7 Gy (Henderson, 1990). Based on their experimental dose measurements, Owen *et al.* (2006) have more recently recommended an absorbed dose limit of 3 × 10^7 Gy for typical macromolecular crystallography experiments.

2.5. Data processing

Data were processed using the *HKL*-2000 software. Each 10° run was individually indexed and the reflections were integrated and scaled. The common reflections among the seven data sets from each crystal were used to calculate the decay in intensities. The sorting of the common reflections was performed using the Microsoft *Access* program. By using only common reflections in the analysis, any effects of inconsistent overflows or partially measured reflections were eliminated. The reflections were then split into sinθ/λ shells of equal thickness and the decay in average signal to noise and intensities [$\langle I/\sigma(I)\rangle$, $\langle I\rangle$] in the same shells for different crystals and different temperatures were compared. The lowest resolution shells (0.0–0.05 and 0.05–0.1 $Å^{-1}$) were merged to increase the number of reflections. For ease of comparison, $\langle I/\sigma(I)\rangle$ and $\langle I\rangle$ in each shell was normalized with respect to the initial data set to calculate a percentage decay. By normalizing the data, valid crystal and temperature comparisons can be made. Other parameters such as mosaicity and unit-cell volume were followed for each cycle.

3. Results

Figs. 1(*a*) and 1(*b*) show normalized $\langle I/\sigma(I)\rangle$ for a consistent set of observed reflections for each cycle in different sinθ/λ

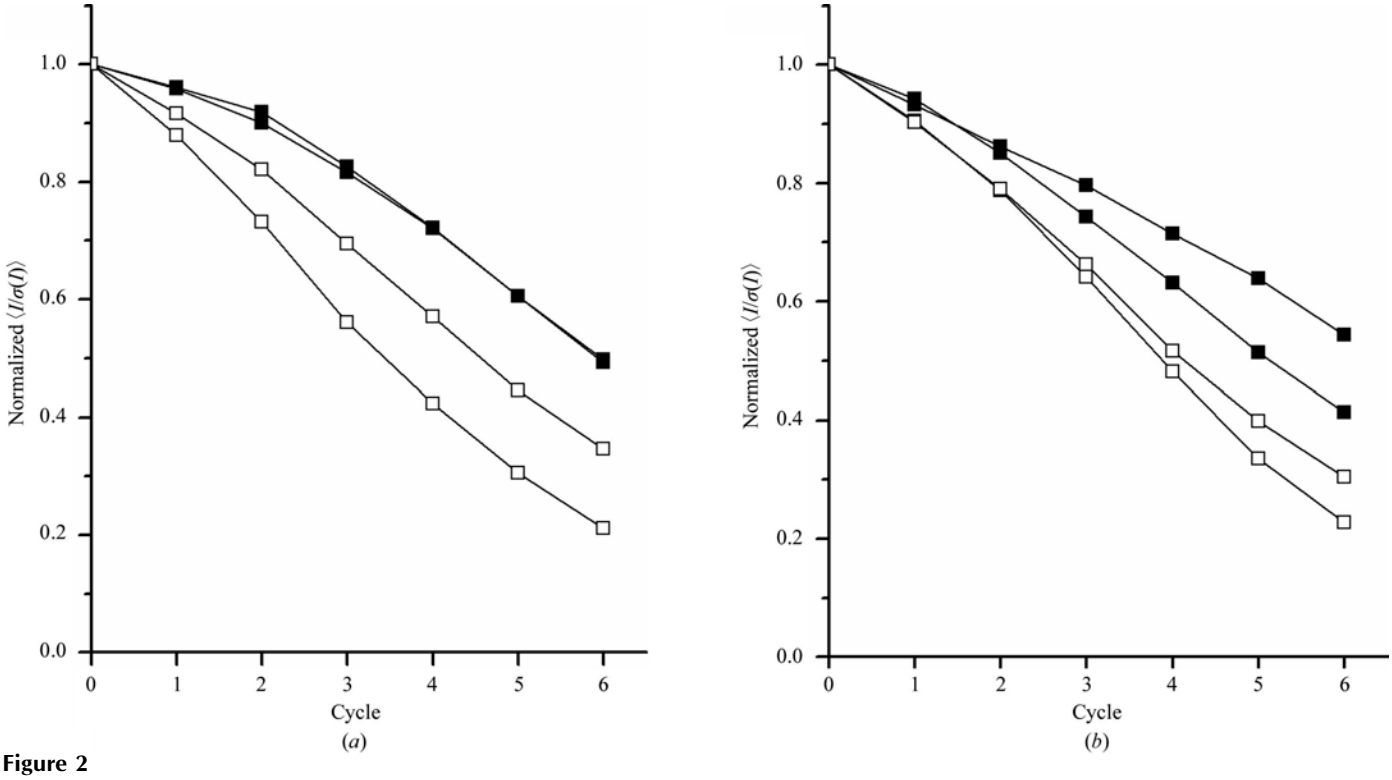

Figure 2
Closed symbols represent data collected with 8 K helium and open symbols represent data collected with 100 K nitrogen. (*a*) Normalized $\langle I/\sigma(I)\rangle$ in the 0.25–30 $Å^{-1}$ (2.0–1.7 Å) shell *versus* number of cycles for four 0.1–0.2 mm crystals. (*b*) Normalized $\langle I/\sigma(I)\rangle$ in 0.3–0.35 $Å^{-1}$ (1.7–1.4 Å) shell *versus* number of cycles for four 0.4–0.5 mm crystals.

shells for a 0.1–0.2 mm crystal at 8 K and a similar crystal at 100 K, respectively. The 8 K helium data consistently exhibit less decay than the 100 K nitrogen data when the same $\sin\theta/\lambda$ shells are compared. For example, the nitrogen data show 79% decay in the initial signal after the sixth cycle in the 0.25–0.3 Å^{-1} shell, while the helium data only show 51% decay in the same shell. Also, the data in the 0.3–0.365 Å^{-1} shell (high-resolution data) disappear [$\langle I/\sigma(I)\rangle$ below 1.5] after the fourth cycle for the nitrogen-cooled crystal, whereas the helium data persist until the sixth cycle, indicating that the use of cryogenic helium leads to a measurable improvement in crystal lifetime. This is perhaps more obvious in Fig. 2(*a*), which compares $\langle I/\sigma(I)\rangle$ *versus* the number of cycles in the 0.25–0.3 Å^{-1} shell for data obtained at 8 and 100 K for 0.1–0.2 mm crystals, and Fig. 2(*b*), which makes the same comparison for the 0.3–0.35 Å^{-1} shell for 0.4–0.5 mm crystals. The crystals cooled with helium decay more slowly than those cooled with nitrogen. Tables and plots of $\langle I/\sigma(I)\rangle$ *versus* $\sin\theta/\lambda$ and $\langle I\rangle$ *versus* $\sin\theta/\lambda$ for all crystals at all temperatures have been deposited[1]. We note that the trends with respect to $\langle I\rangle$ are identical to those of $\langle I/\sigma(I)\rangle$: crystals cooled with He to 8 K decay less rapidly than those cooled with N_2 to 100 K. As in previous studies (Ravelli *et al.*, 2002; Murray & Garman, 2002; Schulze-Briese *et al.*, 2005), changes in unit-cell volume were found to be a poor metric for evaluating radiation damage. Mosaicity changes in XI crystals were not a uniform indicator for either increased dose or damage.

4. Discussion

From Figs. 1 and 2, it is evident that the use of cryogenic helium in place of nitrogen results in additional mitigation of radiation damage and an increase in the crystal lifetime at synchrotron beamlines. The strategy of comparing the same $\sin\theta/\lambda$ sections emphasizes the decay in the signal-to-noise ratio with increasing resolution (higher $\sin\theta/\lambda$), thus demonstrating the importance of resolution-dependent decay corrections. As the reduction in the decay of $\langle I/\sigma(I)\rangle$ at lower temperatures is more prominent in higher resolution shells, the use of helium should be particularly advantageous when collecting high-resolution data.

The mosaicity values for helium-cooled crystals were higher in some cases, which is consistent with results reported by Petrova *et al.* (2006). This may be attributed to the narrow width and high velocity of the helium cryostream. The helium stream used in our experiments is only 2 mm in diameter. Therefore, during the initial crystal alignment the crystal may go off-center and experience thermal stress owing to the radial temperature gradients in the outer part of the stream, especially for large crystals. Also, the higher speed of the helium gas stream in our experiments may cause movement of the cryo-loop, which can partly contribute to the spreading of diffraction spots, although we did not visually observe discernible movement of the loop fibre. Rotella *et al.* (2005) have characterized the effect of loop movement on the observed mosaicities. However, despite higher starting mosaicity values, the He-cooled crystals averaged lower increases in mosaicity during the experiment than did the N_2-cooled crystals.

As a radiation-damage parameter, intensity is not affected by changes in mosaicity, whereas $\langle I/\sigma(I)\rangle$ is correlated to mosaicity. Thus, the average intensity decay would not be expected to precisely match that of $\langle I/\sigma(I)\rangle$. Our choice of $\langle I/\sigma(I)\rangle$ as a metric for radiation damage is based on our desire to use a parameter that can be used as a general and somewhat sensitive measure of radiation damage and can assess the point where diffraction data become unusable (the average signal drops to the level of the noise).

The improvement in crystal lifetime with helium cooling may be attributed to slower diffusion and reactions of free radicals (reduction in secondary-radiation damage) at the lower temperature. This result is in agreement with previous electron-spin resonance experiments on γ-irradiated ice (Kevan *et al.*, 1964; Siegel *et al.*, 1961; Flournoy *et al.*, 1962). Although $H^{\cdot}$ radicals can be generated and observed by irradiation of ice at 4 K, they rapidly disappear on warming (Siegel *et al.*, 1961). Indeed, they are not observed at all in ice irradiated at 77 K, whereas the slower moving $OH^{\cdot}$ radicals are somewhat observable at 77 K (Siegel *et al.*, 1961; Flournoy *et al.*, 1962). These studies were made on crystalline ice, not on a complex solution of amorphous solid water, buffer, precipitant and crystalline protein. The important feature seen in these studies is the reduction in the mobility of radicals derived from water at lower cryogenic temperature.

The temperature at the crystal position is often higher than the set point (in the present case, we measured a temperature of 112 K for a set point of 100 K). Heating of the crystal owing to absorption of the X-ray beam may be responsible for an increase in mobility of free radicals in some cases. Two-dimensional and three-dimensional heat-transfer models for X-irradiated protein crystals have been developed (Kuzay *et al.*, 2001; Kriminski *et al.*, 2003; Nicholson *et al.*, 2001; Mhaisekar *et al.*, 2005) to calculate the temperature rise during data collection at cryogenic temperatures. Such calculations predict a temperature rise of ~5–10 K under a flux density of $\sim10^{14}$ photons s^{-1} mm^{-2}, an order of magnitude greater than that used in our studies. Crystal heating is not expected be significant in our studies; however, radical mobility is expected to be greater in nitrogen-cooled crystals compared with He-cooled crystals.

5. Conclusions and future studies

Our most conservative comparison between similar crystals cooled to different temperatures suggests an extension in crystal diffractive lifetime of 25% (see supplementary data[1]). For the comparison shown in Fig. 1, this value is ~50% (40 min *versus* 60 min of highest resolution shell diffraction). We feel this represents a significant improvement in the lifetime of a diffraction experiment and a significant increase in

[1] Supplementary data have been deposited in the IUCr electronic archive (Reference: SX5058). Services for accessing these data are described at the back of the journal.

data measurement. Two separate analyses of variance (ANOVA) were performed on normalized $\langle I/\sigma(I)\rangle$ for the sixth cycle and the 2.0–1.7 Å shell. The first single-factor ANOVA analysis showed that the average normalized $\langle I/\sigma(I)\rangle$ was statistically significant with respect to temperature [with 99.5% confidence]. The second two-factor ANOVA analysis with replication revealed that the average normalized $\langle I/\sigma(I)\rangle$ was statistically significant with respect to temperature [with a 98.97% confidence] and not significant with respect to crystal size or interaction. A detailed statistical analysis of the decay in intensity [which is much greater than the decay in $\langle I/\sigma(I)\rangle$] will be the subject of future studies.

We attribute the observed improvement in crystal lifetime with helium to decreased free-radical mobility at lower temperatures. These studies provide evidence that the use of helium may be advantageous when collecting data on proteins that are sensitive to radiation damage or when measuring ultrahigh-resolution data that require extended X-ray exposure. When coupled with the potential improvements in resolution and concomitant reduction in atomic thermal parameters (Motoyama *et al.*, 2002; Petrova *et al.*, 2006), helium crystal cooling is an attractive option for data collection, especially at synchrotron beamlines.

Additional benefits may accrue when attempting anomalous dispersive phasing (MAD or SAD) of a novel protein, where completeness and redundancy in the data set are paramount for a successful outcome. As can be seen in Fig. 1, all shells of data participate in the benefits of He crystal cooling. Similar comparative studies to those detailed here are currently under way with XI crystals precipitated with sodium selenate.

Despite frequently expressed concerns with respect to economics (Garman & Owen, 2006), liquid-helium expenditure does not contribute significantly to the cost of a diffraction experiment when measuring diffraction data at a synchrotron. With consumption of 4 l of He per hour, the cost of helium for each crystal in these experiments (∼1 h beam exposure) was US$10 at the APS. Although He is priced much higher elsewhere, the cost of He for a diffraction experiment of a single crystal is trivial compared with the cost of generating a crystal.

Examination of the specific damage to the protein structure at helium and nitrogen temperatures, as well as data measurement at 50 K and neutron diffraction experiments of X-irradiated crystals, may provide further insight into the mechanism of temperature-dependence of radiation damage at cryogenic temperatures. In addition, we are currently examining the enhancement in diffraction lifetime arising from helium cooling as a function of solvent content.

We wish to thank the gracious assistance, advice and financial support of the staff at BioCARS, including Keith Brister (now at Northwestern University), Reinhard Pahl, Robert Henning and Michael Bolbat. Assistance in data measurement was provided by Kristin Kirschbaum and Eric Yearley of the University of Toledo. Use of the Advanced Photon Source was supported by the US Department of Energy, Basic Energy Sciences, Office of Science under Contract No. W-31-109-Eng-38. Use of the BioCARS Sector 14 was supported by the National Institutes of Health, National Center for Research Resources under grant No. RR07707. This research was sponsored by National Aeronautics and Space Administration grant NAG8-1838 (CAS) and by National Science Foundation Grant 466218 (BLH).

References

Burmeister, W. P. (2000). *Acta Cryst.* D**56**, 328–341.
Chinte, U. (2006). PhD thesis. University of Toledo, USA.
Flournoy, J. M., Baum, L. H. & Siegel, S. (1962). *J. Chem. Phys.* **36**, 2229.
Garman, E. (1999). *Acta Cryst.* D**55**, 1641–1653.
Garman, E. & Nave, C. (2002). *J. Synchrotron Rad.* **9**, 327–328.
Garman, E. & Owen, R. L. (2006). *Acta Cryst.* D**62**, 32–47.
Garman, E. F. & Schneider, T. R. (1997). *J. Appl. Cryst.* **30**, 211–237.
Hanson, B. L., Harp, J. A., Kirschbaum, K., Parrish, D. A., Timm, D. E., Howard, A., Pinkerton, A. A. & Bunick, G. J. (2001). *J. Cryst. Growth*, **232**, 536–544.
Hanson, B. L., Harp, J. M., Kirschbaum, K., Schall, C. A., DeWitt, K., Howard, A., Pinkerton, A. A. & Bunick, G. J. (2002). *J. Synchrotron Rad.* **9**, 375–381.
Hanson, B. L., Martin, A., Harp, J. M., Parrish, D. A., Bunick, C. G., Kirschbaum, K., Pinkerton, A. A. & Bunick, G. J. (1999). *J. Appl. Cryst.* **32**, 814–820.
Hanson, B. L., Schall, C. A. & Bunick, G. J. (2003). *J. Struct. Biol.* **142**, 77–87.
Hardie, M. J., Kirschbaum, K., Martin, A. & Pinkerton, A. A. (1998). *J. Appl. Cryst.* **31**, 815–817.
Henderson, R. (1990). *Proc. R. Soc. London B*, **241**, 6–8.
Hope, H. (1988). *Acta Cryst.* B**44**, 22–26.
Kevan, L., Moorthy, P. N. & Weiss, J. J. (1964). *J. Am. Chem. Soc.* **86**, 771–776.
Kriminski, S., Kazmierczak, M. & Thorne, R. E. (2003). *Acta Cryst.* D**59**, 697–708.
Kuzay, T., Kazmierczak, M. & Hsieh, B. J. (2001). *Acta Cryst.* D**57**, 69–81.
Mhaisekar, A., Kazmierczak, M. J. & Banerjee, R. (2005). *J. Synchrotron Rad.* **12**, 318–328.
Motoyama, T., Nakasako, M. & Yamaguchi, I. (2002). *Acta Cryst.* D**58**, 148–150.
Murray, J. & Garman, E. (2002). *J. Synchrotron Rad.* **9**, 347–354.
Murray, J. W., Garman, E. F. & Ravelli, R. B. G. (2004). *J. Appl. Cryst.* **37**, 513–522.
Nave, C. (1995). *Radiat. Phys. Chem.* **45**, 483–490.
Nave, C. & Garman, E. F. (2005). *J. Synchrotron Rad.* **12**, 257–260.
Nicholson, J., Nave, C., Fayz, K., Fell, B. & Garman, E. (2001). *Nucl. Instrum. Methods Phys. Res. A*, **467–468**, 1380–1383.
O'Neill, P., Stevens, D. L. & Garman, E. F. (2002). *J. Synchrotron Rad.* **9**, 329–332.
Owen, R. L., Rudino-Pinera, E. & Garman, E. F. (2006). *Proc. Natl Acad. Sci. USA*, **103**, 4912–4917.
Petrova, T., Ginell, S., Mitschler, A., Hazemann, I., Schneider, T., Cousido, A., Lunin, V. Y., Joachimiak, A. & Podjarny, A. (2006). *Acta Cryst.* D**62**, 1535–1544.
Ravelli, R. B. G. & McSweeney, S. M. (2000). *Structure*, **8**, 315–328.
Ravelli, R. B. G., Theveneau, P., McSweeney, S. & Caffrey, M. (2002). *J. Synchrotron Rad.* **9**, 355–360.
Rodgers, D. W. (1994). *Structure*, **2**, 1135–1140.
Rotella, F. J., Alkire, R. W. & Duke, N. E. C. (2005). *Acta Cryst.* A**61**, C137.
Schulze-Briese, C., Wagner, A., Tomizaki, T. & Oetiker, M. (2005). *J. Synchrotron Rad.* **12**, 261–267.

Sharpatyi, V. A. (1995). *High Energ. Chem.* **29**, 77–90.
Siegel, S., Flournoy, J. M. & Baum, L. H. (1961). *J. Chem. Phys.* **34**, 1782–1788.
Sliz, P., Harrison, S. C. & Rosenbaum, G. (2003). *Structure*, **11**, 13–19.
Teng, T.-Y. & Moffat, K. (2000). *J. Synchrotron Rad.* **7**, 313–317.
Teng, T.-Y. & Moffat, K. (2002). *J. Synchrotron Rad.* **9**, 198–201.
Turner, J. E. (1992). *Atoms, Radiation and Radiation Protection.* New York: McGraw–Hill.
Weik, M., Berges, J., Raves, M. L., Gros, P., McSweeney, S., Silman, I., Sussman, J. L., Houee-Levin, C. & Ravelli, R. B. G. (2002). *J. Synchrotron Rad.* **9**, 342–346.
Weik, M., Ravelli, R. B., Kryger, G., McSweeney, S., Raves, M. L., Harel, M., Gros, P., Silman, I., Kroon, J. & Sussman, J. L. (2000). *Proc. Natl Acad. Sci. USA*, **97**, 623–628.
Weik, M., Ravelli, R. B. G., Silman, I., Sussman, J. L., Gros, P. & Kroon, J. (2001). *Protein Sci.* **10**, 1953–1961.